Conformational Free Energies of 1,2-Dichloroethane in Nanoconfined Methanol

J. A. Gomez,[†] Ashley K. Tucker,[‡] Tricia D. Shepherd,[‡] and Ward H. Thompson*[,†]

Department of Chemistry, University of Kansas, Lawrence, Kansas 66045, and Department of Chemistry/ Physics, Westminster College, Salt Lake City, Utah 84105

Received: April 25, 2005; In Final Form: July 20, 2005

Monte Carlo simulations have been used to construct free energy surfaces of 1,2-dichloroethane dissolved in methanol confined in hydrophobic spherical cavities of varying size (10−15 Å) and solution density (0.6−0.79 g/cm^3). The free energy surfaces are functions of two variables: the (center-of-mass) distance from the cavity wall of 1,2-dichloroethane and the Cl−C−C−Cl dihedral angle. Umbrella sampling and the weighted histogram analysis method were used to obtain accurate results for the free energy in these two degrees of freedom. Our results indicate that the conformational equilibrium and the barrier to internal rotation of the 1,2-dichloroethane depend on the position in the cavity. The results are discussed in the context of the solvent density, orientational distributions, and packing effects.

1. Introduction

Chemistry in nanoconfined solvents has recently been attracting increasing attention. One example is reactivity in microporous and mesoporous catalysts where conformational dynamics and energetics can affect both catalyst activity and selectivity.[1,2] Another is molecular switches, currently of significant interest as components of potential data storage devices. One class of switches is based on photoinduced cis−trans isomerization[3] which may be strongly affected by confinement. Finally, there has recently been increasing interest in the effect of the restricted environment that is found in realistic biological conditions on protein folding.[4] Ideally, one wishes to control the chemistry in these systems not only by manipulating what species are allowed in the cavity but also by designing the cavity properties (or to understand how nature does it). Specifically, confined solvent systems may favor certain reaction pathways and disfavor others, thereby promoting, e.g., selectivity in catalysis or molecular switches that are more resistant to fatigue. However, our understanding of these effects of nanoscale confinement and how they are modified by the cavity characteristics is limited.

In this paper we present an investigation of the free energies of 1,2-dichloroethane (DCE) in methanol confined in spherical, hydrophobic cavities. The DCE molecule is a prototypical test system for conformational equilibrium and has been the subject of a number of theoretical and experimental studies in bulk liquids.[5−19] The trans-gauche isomerization of DCE is relatively facile in the gas phase and bulk solvents, with a barrier of ∼3 kcal/mol.[10] However, the conformational equilibrium is sensitive to the solvent polarity[13] since $\mu_{trans} = 0$ and $\mu_{gauche} \sim 3.5$ D.[17] Thus, the isomerization must involve both changes in the solvent polarization and rearrangement of the solvent to accommodate a change in the molecule shape. The conformational rearrangements should therefore depend strongly on the characteristics of the cavity including the size, shape, dimensionality, and surface functionality through both solute−cavity and solute−solvent interactions. The latter are significant since nanoscale confinement changes both the solvent structure and dynamics.[20−44] The equilibrium and reaction rate constants therefore probe the static and dynamic properties of the solvent including both electrostatic and steric contributions. In addition, in Monte Carlo simulations we have found significantly different position distributions for solutes with different dipole moments[40−42] and molecular dynamics simulations indicate that solute motion in the cavity can be part of the reaction coordinate for solvent-coupled reactions.[43,44] Thus, we present free energy surfaces here as a function of the Cl−C−C−Cl dihedral angle and the DCE molecule position in methanol confined inside hydrophobic spherical nanocavities. These simulations represent a first attempt to examine confinement effects on conformational equilibria in simplistic cavity systems and will serve as a "baseline" for studies of the conformational dynamics and more complex confining frameworks.

There has been little previous experimental or theoretical work on conformational equilibria and dynamics in nanoconfined solvents. One study relevant to this work is that of Luo and Jonas on the trans-gauche conformational equilibrium of ethylene glycol in hydrophilic and hydrophobic sol−gel pores of radii ∼30−70 Å and the bulk.[32] They found the fraction of trans conformer increased as the pore radius decreased for hydroxyl-terminated pores but was essentially constant (and equal to the bulk value) for methyl-terminated pores. They attributed this to hydrogen bonding of ethylene glycol with the pore walls and estimated that the fraction of trans conformers in the layer nearest the wall was ∼0.97.

The remainder of the paper is organized as follows. The interaction potentials for the 1,2-dichloroethane solute, the methanol solvent, and the cavity are described in Section 2. The details of the Monte Carlo simulations and umbrella sampling approach are given in Section 3. Results for the free energy surfaces for DCE in nanoconfined methanol are presented in Section 4. They are discussed in Section 5 in the context of the solvent radial densities and solute orientational distributions. Finally, some conclusions are offered in Section 6.

* To whom correspondence should be addressed.
[†] University of Kansas.
[‡] Westminster College.

10.1021/jp052148g CCC: $30.25
Published on Web 08/27/2005

TABLE 1: The Parameters for the Interaction Models of the Solute and Solvent Molecules Used in the Monte Carlo Simulations[a]

site	ϵ (kcal/mol)	σ (Å)	q	m (g/mol)
solute				
CHD[46]	0.1141	3.98	+0.25	15
Cl	0.2816	3.64	−0.25	35
solvent				
CH_3	0.2072	3.77	+0.265	15
O	0.1701	3.07	−0.700	16
H	0.0000	0.00	+0.435	1

[a] The parameters ϵ and σ define the Lennard-Jones interactions, q the site charge, and m the mass of the atom or group.

2. Interaction Potentials

We have performed Monte Carlo simulations for a 1,2-dichloroethane solute molecule dissolved in methanol solvent confined in hydrophobic spherical cavities. The solute is represented by a model that allows changes in the Cl−C−C−Cl dihedral angle yielding a variety of dipole moments.[45] The geometry of the solute is as follows: the C−C and Cl−C bond distances are 1.53 and 1.78 Å, respectively, and the Cl−C−C angles are both equal to 109.5°. The CHD group is considered as a single unified atom.[46] The solvent methanol is treated as a rigid molecule with the C−O and O−H bonds equal to 1.42 and 0.95 Å, respectively, and the C−O−H angle equal to 108.5°. Here the methyl group (CH_3) is also considered as a unified atom.

In the Monte Carlo simulations, the total energy of the solution confined in a spherical cavity is calculated as the sum of all pairs of solvent−solvent and solute−solvent interactions, the interactions of the solvent and solute molecules with the cavity wall, and the torsional intramolecular energy of the solute. The solvent−solvent and solute−solvent interactions consist of Lennard-Jones and Coulomb potentials while the solute−wall and solvent−wall interactions involve only Lennard-Jones contributions.[34−36] Thus, the expression for the total potential energy for a system of N molecules confined in a cavity may be expressed as,

$$V_{\text{total}}(\boldsymbol{R}) = \sum_{i=1}^{N-1}\sum_{j>1}^{N}\sum_{\alpha_i=1}^{n_i}\sum_{\alpha_j=1}^{n_j} V_{\text{MM}}(r_{\alpha_i\alpha_j}) + \sum_{i=1}^{N}\sum_{\alpha_i=1}^{n_i} V_{\text{WM}}(\boldsymbol{r}_{\alpha_i}) + V_{\text{S}}(\phi) \quad (1)$$

where n_i is the number of atoms (or interaction sites) in molecule i, $r_{\alpha_i\alpha_j}$ denotes the distance between atoms α_i and α_j on molecules i and j, and $\boldsymbol{r}_{\alpha_i}$ denotes the position of atom α_i with respect to the center of the cavity. The first summation gives the contributions due to the intermolecular interactions in which the term $V_{\text{MM}}(r_{\alpha_i\alpha_j})$ represents the Lennard-Jones and Coulomb potential energy of the interaction between atom α_i of molecule i and atom α_j of molecule j and is given by the following equation,

$$V_{\text{MM}}(r_{\alpha_i\alpha_j}) = 4\epsilon_{\alpha_i\alpha_j}\left[\left(\frac{\sigma_{\alpha_i\alpha_j}}{r_{\alpha_i\alpha_j}}\right)^{12} - \left(\frac{\sigma_{\alpha_i\alpha_j}}{r_{\alpha_i\alpha_j}}\right)^{6}\right] + \frac{q_{\alpha_i}q_{\alpha_j}}{r_{\alpha_i\alpha_j}} \quad (2)$$

where $\sigma_{\alpha_i\alpha_j}$ and $\epsilon_{\alpha_i\alpha_j}$ represent, respectively, the Lennard-Jones diameter and well-depth parameter and q_{α_i} is the charge of atom α_i on molecule i. The model parameters for the solute and solvent molecules are given in Table 1. The second summation in eq 1 gives the interaction between solution molecules and the cavity wall. For the Lennard-Jones potential of this interaction, we employed the model developed by Linse and Halle.[35,36]

TABLE 2: The Number of Molecules, N, in the Nanocavity Is Given for Three Densities as a Function of the Cavity Radius[a]

cavity radius (Å)	N		
	0.60 g/cm^3	0.70 g/cm^3	0.79 g/cm^3
10	31	36	41
12		68	
15		143	

[a] The number includes the solvent molecules and the single solute molecule.

This potential depends only on the radial distance of the atom position from the center of the cavity. We used the same parameters as in ref 36: $\sigma_{\text{Wall}} = 2.5$ Å, $\epsilon_{\text{Wall}} = 0.46$ kcal/mol. Finally, the third term in eq 1 is the potential energy of the internal rotation around the C−C bond in the 1,2-dichloroethane molecule and is given by the expression

$$V_{\text{S}}(\phi) = {}^1/_2[V_1(1+\cos\phi) + V_2(1-\cos 2\phi) + V_3(1+\cos 3\phi)] \quad (3)$$

where the V_1, V_2, and V_3 have the values 1.933, −0.333, and 2.567 kcal/mol, respectively. This potential was derived by Jorgensen et al.[5] in the simulation of liquid 1,2-dichloroethane by fitting the available experimental data for the trans-to-gauche and gauche-to-gauche barriers and the energy difference between the trans and gauche conformations.

3. Monte Carlo Simulations

We have carried out Monte Carlo simulations to obtain the radial densities of the solvent and free energies of the solute. All simulations were carried out at a temperature of 298 K using the Metropolis sampling procedure. We have considered cavities with radii $R_{\text{cav}} = 10$, 12, and 15 Å and a solution density of 0.7 g/cm^3. For the cavity with 10 Å, we have also investigated solution densities of 0.6 and 0.79 g/cm^3. The number of molecules for each cavity size and solution density are given in Table 2.[47]

In each Monte Carlo simulation, the confined solution is initiated from a bulk configuration large enough to select the number of desired molecules, N. The initial cavity size is made large enough to include N molecules (typically with dimensions larger than the desired cavity radius). The initial cavity radius is then reduced in the equilibration stage by 0.1 Å every 100 cycles (1 cycle = N steps) until the cavity reaches the desired size. The equilibration continues until a total of 400 000 cycles is completed. Subsequently, 6 000 000 cycles are used for the data collection period for obtaining the solvent density (see below for details of the free energy calculations). When the solute molecule is selected in a Monte Carlo step a random change of the dihedral angle ϕ is performed in addition to rotation and translation. The step sizes for the translational and rotational moves were chosen to yield an approximate acceptance rate of 50%.

To obtain the probability density distribution and free energy of the 1,2-dichloroethane molecule as a function of the (center-of-mass) distance from the cavity wall and Cl−C−C−Cl dihedral angle, we employed the umbrella sampling method[48,49] combined with the weighted histogram analysis method (WHAM) of Kumar et al.[50] Here, we will give a brief description of the method we used for calculating free energies; for further details see refs 50 and 51.

In umbrella sampling a biasing potential, $V^i_{\text{umb}}(\xi(\boldsymbol{R}))$, is added to the potential of the system $V(\boldsymbol{R})$ to concentrate the

sampling in a desired region of configuration space. Here, $\xi(\boldsymbol{R})$ is some general coordinate that may depend on several degrees of freedom. We performed a series of simulations adding biasing potentials in different regions of the configuration space or "windows". In each simulation, biased solute density distributions are constructed in the form of histograms that can then be pieced together.

In a canonical ensemble for a system of N molecules at a constant temperature T and volume, the average biased solute density distribution along the coordinate ξ_o with total potential energy $V(\boldsymbol{R}) + V^i_{\text{umb}}(\xi(\boldsymbol{R}))$ is given by,

$$P^i_{\text{biased}}(\xi_o) = \frac{e^{-\beta V^i_{\text{umb}}(\xi_o)} P^i_{\text{unbiased}}(\xi_o)}{\langle e^{-\beta V^i_{\text{umb}}(\xi(\mathbf{R}))} \rangle_{\text{unbiased}}} \tag{4}$$

where $\beta = 1/k_B T$, k_B is Boltzmann's constant, $P^i_{\text{unbiased}}(\xi_o)$ is the solute density distribution in the unbiased system but accurate only in a restricted region of the cavity determined by the biased potential, and the denominator is an average computed with the unbiased potential. We carried out a set of M simulations at the same temperature T with different biasing potentials $V^i_{\text{umb}}(\xi(\boldsymbol{R}))$, $i = 1, M$.

The reconstruction of the full unbiased solute density distribution $P(\xi_o)$ from the separate biased distributions $P^i_{\text{biased}}(\xi_o)$ is based on the weighted histogram analysis method. The WHAM equations employed to compute the complete, unbiased solute density distribution are

$$P(\xi_o) = \frac{\sum_{i=1}^{M} m_i P^i_{\text{biased}}(\xi_o)}{\sum_{i=1}^{M} m_i e^{-\beta[V^i_{\text{umb}}(\xi_o) - f_i]}} \tag{5}$$

and

$$e^{-\beta f_i} = \int d\xi_o \, P(\xi_o) \, e^{-\beta V^i_{\text{umb}}(\xi_o)} \tag{6}$$

where f_i is the window free energy of the ith biased simulation and represents the shift needed to make the unbiased solute density distribution continuous; m_i is the length of the i th simulation, i.e., the number of configurations or steps used to compute $P^i_{\text{biased}}(\xi_o)$. These equations provide a way to compute the density distribution $P(\xi_o)$ and thereby the free energy. Since $P(\xi_o)$ and the set of free energies f_i are unknown initially, these equations must be solved iteratively.

We have used biasing potentials in two variables: the distance from the center of the cavity of the center-of-mass position (r) and the Cl−C−C−Cl dihedral angle (ϕ) of the solute molecule. The biasing potential is written as,

$$V^i_{\text{umb}}(r,\phi) = {}^1/_2 k_r (r - r^i)^2 + {}^1/_2 k_\phi (\phi - \phi^i)^2 \tag{7}$$

where k_r and k_ϕ are force constants and r^i and ϕ^i are reference values of the coordinates for the ith simulation. With the biasing potential of eq 7, we can generate the biased probability distribution $P^i_{\text{biased}}(r,\phi)$ concentrated around the reference coordinate (r_i,ϕ_i). We have obtained the full unbiased probability density $P(r,\phi)$ by solution of eqs 5 and 6. The (Helmholtz) free energy is obtained from the full unbiased probability density as,

$$A(r,\phi) = -k_B T \ln P(r,\phi) \tag{8}$$

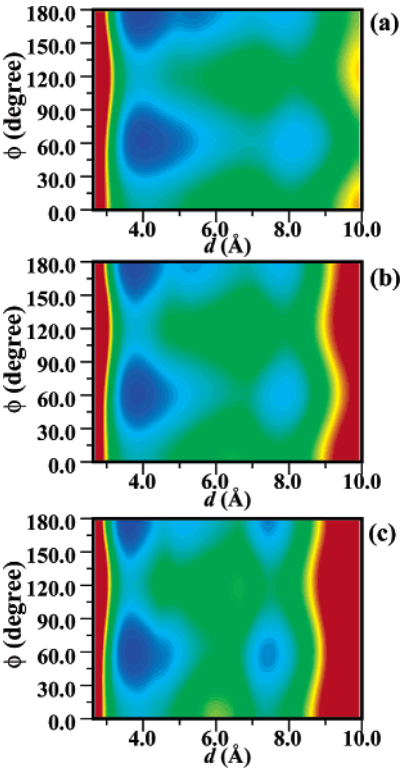

Figure 1. The free energy is plotted as a function of the (center-of-mass) distance from the cavity wall, d, and the Cl−C−C−Cl dihedral angle, ϕ, for $R_{\text{cav}} = 10$ Å and a solution density of (a) 0.6, (b) 0.7, and (c) 0.79 g/cm^3. In each plot 60 contours are shown between the lowest (blue, 0.0 kcal/mol) and highest (red, 11.0 kcal/mol) values considered for the free energy.

The values used for the force constants were $k_r = 160.0$ kJ/mol/Å^2 and $k_\phi = 0.012$ kJ/mol/deg^2 in all the simulations. The reference values of the coordinates r^i and ϕ^i were separated by 0.25 Å and 20.0°, respectively. Each Monte Carlo simulation to calculate the biased solute density distribution, $P^i_{\text{biased}}(r,\phi)$, consisted of 400 000 equilibration cycles and 4 000 000 cycles.

Error bars for the free energies for $R_{\text{cav}} = 10$ Å ($\rho = 0.6$ and 0.7 g/cm^3) have been obtained by using block averaging.[48] Specifically, the configurations from the umbrella sampling Monte Carlo simulations have been saved every 10 cycles and the standard deviation for the free energy calculated using eight blocks; the uncertainty is taken to be this block-averaged standard deviation divided by $\sqrt{N_{\text{blocks}}}$. Test calculations for $R_{\text{cav}} = 12$ Å indicate the error does not depend strongly on cavity size (an expected result since the density of biasing potentials positions is the same).

4. Free Energy Surfaces

Free energy contour plots for the solute molecule as a function of the (center-of-mass) distance from the cavity wall, d, and the Cl−C−C−Cl dihedral angle, ϕ, are shown in Figure 1. These free energy surfaces were obtained as described in Section 3 for a 10 Å radius cavity and solution densities of 0.6, 0.7, and 0.79 g/cm^3. The effect of cavity size on the free energies is shown in Figure 2 where free energy surfaces are presented for cavities of radius 10, 12, and 15 Å and a solution density of 0.70 g/cm^3. The most general feature from these figures is that the DCE solute has local conformational minima near $\phi \simeq 60°$ and 180°, i.e., the gauche and trans conformations, independent of the cavity size and solution density. A number of other features are also evident which we now discuss.

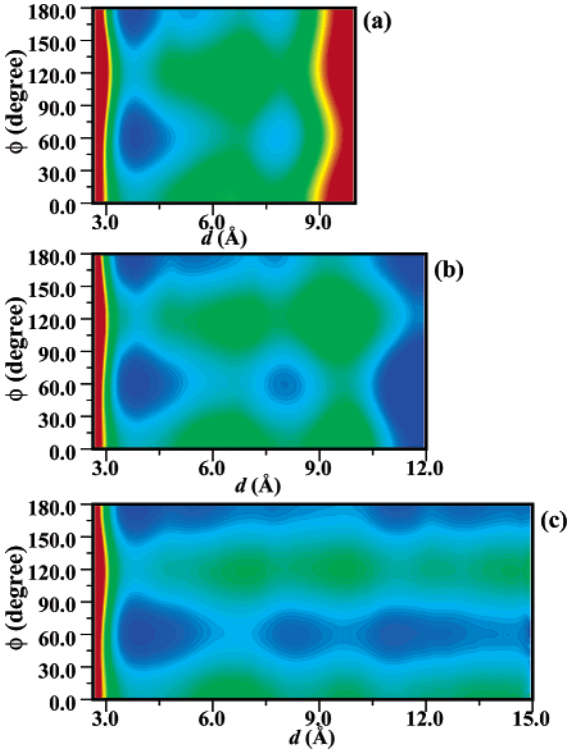

Figure 2. Same as Figure 1 but results are shown for a solution density of 0.7 g/cm^3 and a cavity radius of (a) 10, (b) 12, and (c) 15 Å. Also, in panel b, the range of contours is −2.2 to 13.2 kcal/mol.

4.1. R_{cav} = 10 Å, ρ = 0.6, 0.7, and 0.79 g/cm^3. We first consider the results for the smallest cavities. One notable feature of the free energy surfaces in Figure 1 is that there are two local minima in the DCE center-of-mass coordinate for the gauche configuration but three for the trans conformer. This is observed for all three solution densities considered. However, as the solution density is increased the wells become narrower as the barriers between the minima increase. The relative free energies of these minima with respect to the corresponding global minimum (which is found to be the trans conformation located nearest the cavity wall) are given in Table 3 along with the minima locations; uncertainties in the free energy are given for ρ = 0.6 and 0.7 g/cm^3 based on the block-averaged standard deviation as described in Section 3.

The results presented in Table 3 show that the positions of the minima are shifted toward the cavity wall as the solution density increases. (The origin of these shifts lies in the arrangement of the solvent molecules in the cavity as discussed below in Section 5.1 where the solvent radial densities are presented.) In addition, we can see that the most stable position for both the gauche and trans conformers is near the cavity wall. The precise locations of the minima are slightly different for the two conformers, however, with the center-of-mass of the trans conformer ∼0.1 Å closer to the cavity wall. As noted above, the trans conformer has a lower free energy than the gauche near the cavity wall but by only a small amount: 0.1−0.27 kcal/mol; this energy difference decreases as the solvent density increases. (It is also worth noting that the statistical errors in the free energy increase with distance from the cavity wall, i.e., away from the global minimum, but depend only very weakly on the solution density.)

The trans conformation has a local minimum not observed for the gauche conformer at $d \sim 5.1-5.3$ Å. As will be discussed in greater detail in Section 5.2, this local minimum corresponds to a different orientation of the DCE molecule relative to the cavity wall than the other two minima; this orientation is not favorable for the gauche conformer. The free energy of this minimum is raised as the solvent density is increased: it is 1.17, 1.67, and 1.87 kcal/mol for ρ = 0.6, 0.7, and 0.79 g/cm^3, respectively.

For the local minimum nearest the cavity center, $d \sim 7.4-8.1$ Å, the minimum for the trans conformer is located slightly nearer the cavity wall than that for the gauche form for all the solution densities. Interestingly, the free energy of this minimum (relative to the global minimum) is greatest for ρ = 0.7 g/cm^3 and lowest for ρ = 0.79 g/cm^3. In addition, the gauche conformer is more stable than the trans except for the highest solution density of 0.79 g/cm^3. This is consistent with previous simulations that indicate the effective solvent polarity is greater in the cavity interior than near the cavity wall since the more polar gauche form is stabilized relative to the trans conformer (which has no net dipole moment).

We have used the probability distributions corresponding to the free energy surfaces in Figure 1 to calculate the total fraction of trans and gauche conformers in the cavity. Specifically, we integrated the probability distribution over all positions in the cavity and ϕ between 0 and 120° to obtain the fraction of conformers that are gauche, f_G. The fraction of DCE conformers that are trans is $f_T = 1 - f_G$. The results show that the trans conformer is less favored as the solvent density increases. That is, f_T = 0.41, 0.37, and 0.31 for ρ = 0.6, 0.7, and 0.79 g/cm^3, respectively. This indicates that the effective solvent polarity increases with solution density.

4.2. R_{cav} = 10, 12, and 15 Å, ρ = 0.7 g/cm^3. In Figure 2, we can see that the number of local minima increases as the cavity size increases. For the trans conformer (ϕ = 180°) we can distinguish four and five minima for cavities with radii of 12 (Figure 2b) and 15 Å (Figure 2c), respectively, while for the gauche conformer ($\phi \simeq 60°$) three and four minima are found for cavities with radii of 12 (Figure 2b) and 15 Å (Figure 2c), respectively. In addition, we can see that the barriers between

TABLE 3: Relative Free Energies of the Minima (with respect to the global minimum) Are Given for 1,2-Dichloroethane in Methanol for R_{cav} = 10 Å and Three Solution Densities[a]

	trans			gauche		
ρ (g/cm^3)	ΔA_{min} (kcal/mol)	ϕ_{min} (deg)	d_{min} (Å)	ΔA_{min} (kcal/mol)	ϕ_{min} (deg)	d_{min} (Å)
0.60	0.00 ± 0.03	180.0	3.9	0.27 ± 0.01	63.0	4.0
	1.17 ± 0.04	180.0	5.3			
	1.92 ± 0.09	180.0	7.8	1.84 ± 0.07	61.0	8.1
0.70	0.00 ± 0.03	180.0	3.8	0.21 ± 0.02	60.1	3.8
	1.67 ± 0.06	180.0	5.3			
	2.15 ± 0.10	180.0	7.7	2.04 ± 0.08	61.7	7.9
0.79	0.00	180.0	3.6	0.10	60.1	3.7
	1.87	180.0	5.1			
	1.41	180.0	7.4	1.47	57.5	7.4

[a] Here, d is the (center-of-mass) distance of the DCE from the cavity wall and ϕ is the Cl−C−C−Cl dihedral angle.

TABLE 4: Same as Table 3, but Here Results Are Shown for $\rho = 0.7$ g/cm^3 and Three Different Cavity Radii[a]

	trans			gauche		
R_{cav} (Å)	ΔA_{min} (kcal/mol)	ϕ_{min} (deg)	d_{min} (Å)	ΔA_{min} (kcal/mol)	ϕ_{min} (deg)	d_{min} (Å)
10	0.00 ± 0.03	180.0	3.8	0.21 ± 0.02	60.1	3.8
	1.67 ± 0.06	180.0	5.3			
	2.15 ± 0.10	180.0	7.7	2.04 ± 0.08	61.7	7.9
12	0.00	180.0	3.8	0.03	61.0	3.8
	1.15	180.0	5.5			
	1.54	180.0	7.8	1.26	59.4	8.0
	−0.74	180.0	11.7	−2.2	57.1	11.9
15	0.00	180.0	3.8	0.13	61.6	3.9
	0.67	180.0	5.4			
	1.20	180.0	7.7	0.93	59.2	8.3
	0.64	180.0	11.3	0.74	59.3	11.1
	0.90	180.0	13.3	1.05	60.3	12.3

[a] The global minimum is taken to be the trans conformer minimum nearest the cavity wall for all cavity sizes, even though this is not the case for $R_{cav} = 12$ Å; see the text for a discussion of this point.

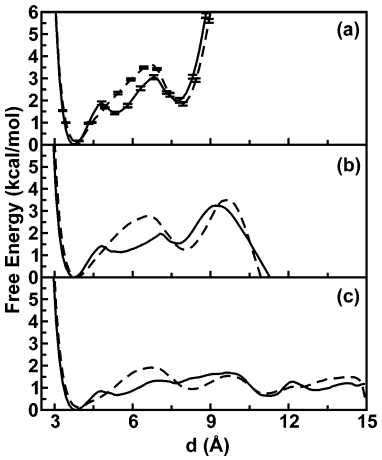

Figure 3. The free energy of 1,2-dichloroethane in nanoconfined methanol is plotted as a function of the (center-of-mass) distance from the cavity wall, d, for fixed values of the dihedral angle, ϕ. (These data are extracted from Figure 2, $\rho = 0.7$ g/cm^3.) The results for $\phi = 180°$ (solid line) and 61° (dashed line) and a cavity of radius (a) 10, (b) 12, and (c) 15 Å are shown.

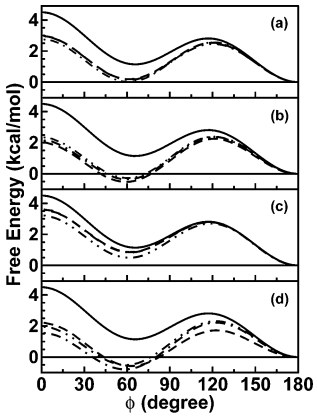

Figure 4. Free energy curves in the Cl−C−C−Cl dihedral angle are shown as obtained from Figure 2 ($\rho = 0.7$ g/cm^3) by taking one-dimensional slices for fixed d. Results are given for d equal to (a) 3.8, (b) 4.56, (c) 5.44, and (d) 8.44 Å. The dashed, dot-dashed, and dot-dot-dashed lines are for cavities with radii of 10, 12, and 15 Å, respectively. For comparison the in vacuo energy is shown as a solid line.

the local minima along the radial coordinate are reduced as the cavity size increases. Thus, it is expected that the solute may diffuse more easily as the cavity size is increased. This feature is further addressed in Section 5.1.

The relative free energy values of the minima with respect to the corresponding global minimum and their coordinates for Figure 2 are given in Table 4. From these values it can be seen that the global minimum for cavities with radii of 10 and 15 Å is when the solute molecule is in the trans conformation near the cavity wall while for the cavity with a radius of 12 Å the solute is most stable in the gauche conformation at $\phi = 57.1°$ near the center of the cavity. As discussed in Section 5.1, the latter case is due to the solute sitting near the center of the cavity giving a large probability due to the small volumes of those histogram bins. The next lowest minimum is the trans conformation near the cavity wall.

To better illustrate the features of the free energy contour plots in Figure 2, we extracted one-dimensional free energy curves for fixed values of the distances from the cavity wall, d, and fixed values of the Cl−C−C−Cl dihedral angle, ϕ. Free energy curves for fixed values of the dihedral angle ($\phi = 61°$ and 180°) are shown in Figure 3 for cavities with radii of 10, 12, and 15 Å. Error bars are given for $R_{cav} = 10$ Å based on the block-averaged standard deviation; as noted in Section 3 test calculations indicate the errors do not depend strongly on cavity size. A number of features can be observed in this figure. First, for $R_{cav} = 10$ Å the presence of two minima for the gauche conformer and three minima for the trans conformer can be clearly seen. Second, an analogous structure in the free energy curves for $R_{cav} = 12$ and 15 Å is found for 3 Å $< d <$ 10 Å. Third, the free energy barriers decrease as R_{cav} increases. Fourth, for the largest cavity the free energy curves for both conformers exhibit oscillations. Fifth, the difference in the trans and gauche conformer free energies means that the most stable conformer depends strongly on the DCE position in the cavity.

This dependence of the lowest free energy structure on the DCE position can also be seen by plotting one-dimensional curves in ϕ for fixed values of d as shown in Figure 4 (extracted from the free energy contour plots in Figure 2) for $d = 3.8$, 4.56, 5.44, and 8.44 Å. For comparison, the free energy curve of 1,2-dichloroethane in vacuo is included. In each curve the zero of energy is taken to be the trans conformation of the solute ($\phi = 180°$). From these curves, we can see that the gauche conformer ($\phi \simeq 60°$) free energy (relative to the trans conformation) is lowered compared to the gas-phase energy independent of the cavity size and position in the cavity. We can also see the alternating behavior of the conformational equilibrium between gauche and trans conformations along the radial coordinate: at $d = 3.8$ and 5.44 Å the trans conformation is more stable and at $d = 4.56$ and 8.44 Å the gauche conformation is more stable. The free energy curves do not depend strongly on cavity size for $d = 3.8$ (Figure 4a) and 4.56 Å (Figure 4b), while for DCE positions further from the cavity wall, $d = 5.44$

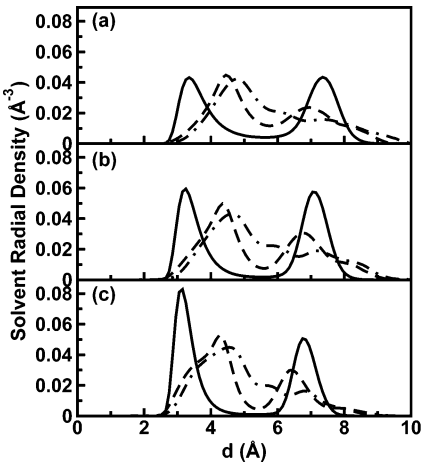

Figure 5. The atomic radial solvent densities are plotted as a function of the distance from the cavity wall, *d*. Results are shown for a cavity of radius 10 Å and solution densities of (a) 0.6, (b) 0.7, and (c) 0.79 g/cm^3. The methyl group (solid line), oxygen atom (dashed line), and hydrogen atom (dot-−dashed line) densities are plotted.

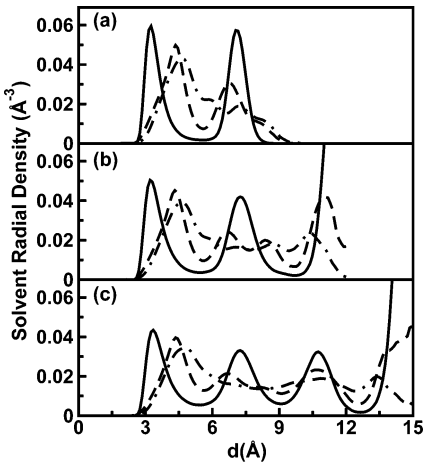

Figure 6. Same as Figure 5 for cavities with radii of (a) 10, (b) 12, and (c) 15 Å and with solution density of 0.7 g/cm^3.

(Figure 4c) and 8.44 Å (Figure 4d), a slightly stronger dependence on R_{cav} is observed.

For 1,2-dichloroethane in the gas phase the trans conformation is favored by 1.2 kcal/mol, and the energy barriers for the gauche-to-gauche and trans-to-gauche transitions are 4.5 and 2.8 kcal/mol, respectively. (The ϕ angles at the minima are 65.1° and 180° for the gauche and trans forms, respectively.) It is also known that this conformational equilibrium is altered upon the solvation with the medium.[5,10,13,14,16] The gauche conformation with a dipole moment of 3.5 D is better stabilized as the polarity of the solvent increases compared to the trans conformation that has no dipole moment by symmetry. From Figure 4, the energy barriers for the gauche-to-gauche and trans-to-gauche conversion are reduced to around 2.8 and 2.5 kcal/mol, respectively, for the free energy curves at $d = 3.8$ Å and around 2.1 and 2.3 kcal/mol, respectively, for $d = 4.56$ Å. The reduction of the gauche-to-gauche and trans-to-gauche barriers can be attributed to better solvation of the solute in the gauche conformation by methanol (through a combination of solvent polarity, orientational, and packing effects). Thus, the solvation of 1,2-dichloroethane in methanol confined in cavities alters the conformational equilibrium and will also affect the kinetics for conformational isomerizations.

As for the $R_{cav} = 10$ Å cases discussed in Section 4.1, we can use the probability distributions corresponding to the free energy surfaces of Figure 2 to determine the total fractions of gauche and trans conformers as a function of cavity size. We find that $f_T = 0.38$, 0.34, and 0.37 for $R_{cav} = 10$, 12, and 15 Å. Thus, the relative gauche and trans populations are relatively independent of cavity size. This is generally consistent with the results of Luo and Jonas for ethylene glycol in hydrophobic sol−gel pores.[32] Naturally, the present system is quite different (spherical cavity rather than pores, atomically smooth walls, solute conformers rather than solvent conformers) but interestingly the results are similar. The effect of changing the cavity surface chemistry (e.g., to be hydrophilic, a case for which Luo and Jonas do see a strong pore size dependence) will be probed in future work.

5. Discussion

5.1. Solvent Radial Densities. The atomic radial densities of the solvent are shown in Figure 5 as a function of the distance from the cavity wall for a cavity of radius 10 Å and solution densities of 0.6, 0.7, and 0.79 g/cm^3. From this figure we can see that the methyl group and oxygen atom densities have two distinct peaks indicating a well-defined layered structure and the hydrogen atom density has one broad peak distributed over most of the cavity. The peaks become narrower and shift toward the cavity wall as the solution density increases. In addition, the peak in the methyl group density nearest the cavity wall increases in height compared to the peak in the cavity interior as the solution density increases. The methyl group displays the strongest layering with the distance between peaks similar to the Lennard-Jones diameter ($\sigma_{CH_3} = 3.77$ Å); this distance decreases as the solution density increases with values of 4.01, 3.80, and 3.61 Å for solution densities of 0.6, 0.7, and 0.79 g/cm^3, respectively.

In Section 4.1, it was observed from the free energy surfaces of DCE in Figure 1 for a cavity of 10 Å radius that as the solution density increases the wells of the local minima become narrower as the barriers between the minima increase. In addition, from Table 3, it was found that the positions of the local minima in the free energy shift toward the cavity wall as the solution density increases. The narrowing of the wells and increasing of the barriers between local minima as the solution density increases is attributed to the corresponding layered structure of the solvent density, i.e., it is expected that diffusion in the radial direction will be inhibited as the solution density increases. The shifting of the local minima in the free energy toward the cavity wall is attributed to the shifting of the solvent molecule layers, i.e, the position of the DCE is correlated with the solvent molecule positions. We can see this feature by comparing Table 3 and Figure 5, generally the local minima are located in the vicinity of the peaks of the solvent density but for the trans conformer an additional local minimum is observed between the peaks ($d \simeq 5.3$ Å). The origin of this minimum is discussed below in Section 5.2.

The atomic densities for the solvent in cavities of radius 10, 12, and 15 Å and $\rho = 0.7$ g/cm^3 are shown in Figure 6. From these data it is clear that the layered structure is primarily associated with the probability density of the methyl group and there are two, three, and four layers for cavities with radii of 10, 12, and 15 Å, respectively. The oxygen radial density also has a layered structure, though less pronounced, while the hydrogen radial density is considerably less structured. The largest maximum in the radial density is found near the cavity wall for all three atoms except for the peaks located at the cavity center for $R_{cav} = 12$ and 15 Å. These peaks are due to a single solvent molecule located near the cavity center (the small

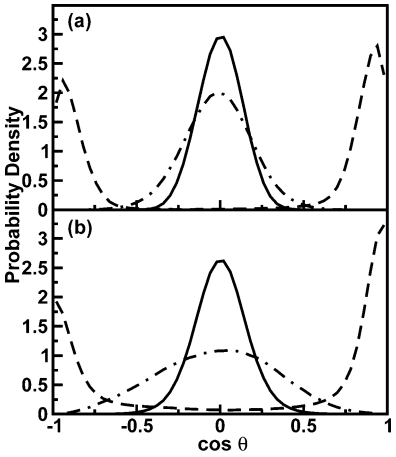

Figure 7. The orientational distributions for the Cl−Cl vector of 1,2-dichloroethane are plotted for the (a) trans and (b) gauche conformations in a cavity of radius 10 Å and solution density 0.7 g/cm^3. Results are shown for restraining the DCE position in the vicinity of $d = 3.8$ (solid line), 5.3 (dashed line), and 7.7 Å (dot-dashed line) for the solute in the trans conformation and $d = 3.8$ (solid line), 5.3 (dashed line), and 7.9 Å (dot-dashed) for the solute in the gauche conformation.

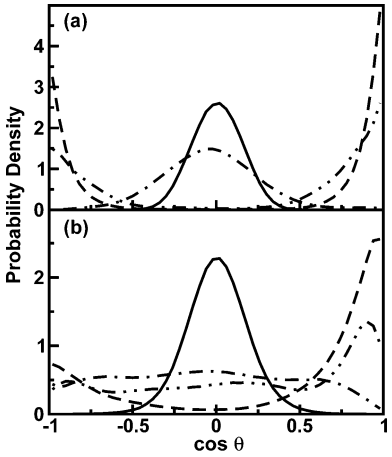

Figure 8. Same as Figure 7 but for a 12 Å radius cavity and results are shown for restraining the DCE position in the vicinity of $d = 3.78$ (solid line), 5.54 (dashed line), 7.8 (dot-dashed line), and 9.4 Å (dot-dot-dashed line) for the trans conformer and $d = 3.81$ (solid line), 5.54 (dashed line), 8.04 (dot-dashed), and 9.4 Å (dot-dot-dashed line) for the gauche conformer.

volume in the histogram bins nearest the center of the cavity gives extremely large densities) with the methyl group closest to the center.[39] It is also observed that as the cavity size increases the layered structure becomes somewhat less pronounced. That is, the peak heights in the radial density are reduced and the minima between peaks are raised. This behavior has been previously observed with a similar solvent (CH_3I) confined in spherical cavities.[43,39] It is expected that the solute molecule may diffuse more easily as the cavity size is increased as a consequence of this,[43] i.e., the barriers to diffusion are reduced as the cavity size increases or the density decreases.

5.2. 1,2-Dichloroethane Orientational Distributions. It was demonstrated in Section 5.1 that the positions of the local minima of the DCE center-of-mass in the free energy surfaces displayed in Tables 3 and 4 are located in the vicinity of the solvent atomic density peaks shown in Figures 5 and 6, respectively. In addition, there is a local minimum for the trans conformer located between the two peaks nearest to the cavity wall (at $d \sim 5.1-5.4$ Å) for all cavity sizes and solution densities considered that is not observed for the gauche conformer. To investigate the origin of these minima further we have constructed orientational distributions for the DCE for (center-of-mass) positions corresponding to the different minima. Specifically, we have calculated orientational distributions for the Cl−Cl vector of DCE with respect to the surface normal of the cavity wall for the trans and gauche conformations. The distributions have been obtained from Monte Carlo simulations with fixed values of the Cl−C−C−Cl dihedral angle corresponding to the gauche (60°) and trans (180°) conformers. The DCE center-of-mass position was constrained in the radial coordinate by using the first term in eq 7.

The orientational distributions of DCE in the trans and gauche conformations are shown in Figures 7 and 8 for cavities with radii of 10 and 12 Å, respectively, and a solution density of 0.7 g/cm^3. The distributions are shown as a function of cos θ, where θ is the angle between the vector from the middle of the Cl−Cl vector to the nearest point on the cavity wall and the Cl−Cl vector. The angle θ is defined such that cos $\theta = \pm 1$ (cos $\theta = 0$) corresponds to the Cl−Cl vector perpendicular (parallel) to the cavity wall.

The DCE center-of-mass positions considered for the 10 Å radius cavity are $d = 3.8$, 5.3, and 7.7 Å for the trans and $d = 3.8$, 5.3, and 7.9 Å for the gauche conformations, i.e., those of the local minima (except the gauche conformer at $d = 5.3$ Å), see Table 4. (Here, d determines r_i in eq 7 by $r_i = R_{cav} - d$.) In a similar manner for the 12 Å radius cavity the positions $d = 3.78$, 5.54, 7.8, and 9.4 Å were chosen for the trans conformer and $d = 3.81$, 5.54, 8.04, and 9.4 Å for the gauche conformer (cf. Table 4). The position at $d = 9.4$ Å is considered because it lies between the peaks in the solvent density (see Figure 6b).

For the 10 Å radius cavity, the orientational distributions shown in Figure 7 for DCE positions corresponding to the local minima in the free energy ($d = 3.8$ and 7.7 Å for trans and $d = 3.8$ and 7.9 Å for gauche) are centered about cos $\theta = 0$ indicating that the Cl−Cl vector is oriented parallel to the cavity wall. When the DCE is restrained in the vicinity of $d = 5.3$ Å we see that the distributions are centered about cos $\theta = \pm 0.94$ and ± 1.0 for the trans and gauche conformations of DCE, respectively, indicating that the solute is oriented nearly perpendicular to the cavity wall. Thus, the picture resulting from these simulations is the following. For the positions $d = 3.8$ and ~7.8 Å the DCE molecule lies primarily parallel to the wall. This means that it sits within a single solvent layer (see Figure 5). In both cases this corresponds to a local minimum in the free energy with the trans conformer slightly more stable near the cavity wall ($d = 3.8$ Å) and the gauche conformer slightly more stable in the cavity interior ($d \sim 7.8$ Å) as shown in Figures 1 and 3a. At the intermediate position ($d = 5.3$ Å) the DCE molecule lines up primarily perpendicular to the cavity wall, corresponding to one CHD-Cl group lying in the solvent layer near the wall and the other CHD-Cl group in the solvent layer near the cavity center. This represents a local minimum for the more extended trans conformation ($r_{Cl-Cl} = 4.3$ Å) but not for the more compact gauche conformation ($r_{Cl-Cl} = 3.2$ Å). (Note that the peaks in the methyl group density are separated by ~3.8 Å.)

The orientational distributions for the DCE Cl−Cl vector for $R_{cav} = 12$ Å and $\rho = 0.7$ g/cm^3 are shown in Figure 8. For the most part, these orientational distributions exhibit analogous features to those for the $R_{cav} = 10$ Å case. Namely, for the local minimum nearest the wall ($d \sim 3.8$ Å) the distributions for both conformers are centered around cos $\theta = 0$ indicating the molecule lies parallel to the cavity wall in the first solvent layer. As for the smaller cavity, the trans conformer is slightly lower in free energy. For the intermediate position ($d = 5.54$

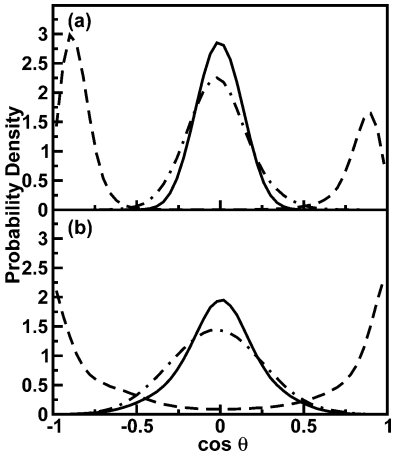

Figure 9. Same as Figure 7 but for simulations with no charges on the 1,2-dichloroethane solute.

Å) the distributions are peaked around cos $\theta \simeq \pm 1$. Thus, the DCE molecule is primarily perpendicular to the wall at this radial position and this is a more favorable arrangement for the trans conformer than the gauche (yielding a local minimum for the former but not the latter). However, for the $d \sim 8$ Å position, the orientational distribution is peaked near cos $\theta = 0$ for the trans conformer but nearly uniform for the gauche conformer. We do not have a full understanding of the origin of this difference; however, it may be due to the less prominent solvent layering in the 12 Å radius cavity that may allow the more compact gauche conformer to orient more freely. Finally, for the position nearest the cavity center ($d = 9.4$ Å) the distributions are peaked near cos$\theta = \pm 1$ for both conformers but broader for the gauche conformer than the trans. Note that $d = 9.4$ Å corresponds to a minimum in the solvent radial density and thus this result is generally consistent with the distributions at $d = 5.54$ Å.

Finally, we address the issue of the origin of this perpendicular orientation of the DCE molecule where the center of mass lies between two solvent layers. In particular, we have investigated whether this orientation is determined predominantly by electrostatic interactions or packing effects. That is, we have recalculated the orientational distributions for $R_{cav} = 10$ Å with no charges on the 1,2-dichloroethane molecule. The results are shown in Figure 9. Comparison of these orientational distributions to those in Figure 7 finds quite small differences. Specifically, the widths of the distributions are slightly altered but the semiquantitative features are all the same. For example, the DCE molecule is still found to lie primarily parallel to the cavity wall for $d = 3.8$ and 7.8 Å, but primarily perpendicular to the cavity wall for $d = 5.3$ Å. Thus, these results show that the Coulombic interactions of the solute are quite unimportant in determining the molecule orientation and indicate that packing effects dominate. On the other hand, the electrostatic interactions almost surely affect the free energy for the DCE molecule oriented perpendicular to the wall which is a local minimum for the trans conformer but not for the gauche. Note that these results are also suggestive of the way in which larger molecules will orient in confined solvent systems.

6. Conclusions

We have performed Monte Carlo simulations to obtain the free energy of 1,2-dichloroethane dissolved in methanol confined in hydrophobic spherical nanocavities of radius 10−15 Å. Free energy surfaces were calculated as a function of the (center-of-mass) DCE distance from the cavity wall and the Cl−C−C−Cl dihedral angle using umbrella sampling. To interpret the results, the solvent radial densities and DCE orientational distributions have also been computed.

The free energy surfaces obtained from the simulations are somewhat complex with several local minima. We have shown that the structure of the free energy surfaces is strongly influenced by the solvent radial density (i.e., how the methanol solvent packs in the nanocavity), which shows significant layering. Both the trans and gauche conformers have local minima corresponding to the DCE molecule lying in each of the solvent layers. In addition, the trans conformer has additional minima at (center-of-mass) positions between solvent layers in which the DCE molecule is aligned perpendicular to the cavity wall with a CH_2-Cl moiety in each layer. We have demonstrated that this perpendicular orientation is primarily due to packing effects and is only weakly affected by the DCE electrostatic interactions. These features of the free energy surfaces indicate that the most stable conformer depends strongly on the position of the DCE molecule in the cavity.

The gauche conformer is preferentially stabilized over the trans conformer in the cavities compared to the gas phase. In particular, the free energy of the gauche conformation relative to the trans is lower the higher the solution density. This is reflected in the dependence of the fraction of conformers that are gauche, which increases for $R_{cav} = 10$ Å as the solution density is increased. In contrast, the gauche free energy and fraction of gauche conformers are relatively independent of cavity size. This is generally consistent with the previous experimental results of Luo and Jonas of neat ethylene glycol in hydrophobic sol−gel pores.[32] In addition, as the cavity size is increased, the layering of the methanol solvent becomes less extreme and the free energy barriers to diffusion of the DCE solute are reduced. These free energy calculations provide an important point of comparison with simulations of the DCE diffusion and conformational isomerization dynamics that we are currently pursuing, particularly in the context of separating energetic and dynamical effects in confined solvent reaction dynamics.

Acknowledgment. The authors thank Prof. Shenmin Li for several useful discussions. This work was supported by the Chemical Sciences, Geosciences and Biosciences Division, Office of Basic Energy Sciences, Office of Science, U.S. Department of Energy. Acknowledgment is made to the donors of the Petroleum Research Fund, administered by the American Chemical Society, for partial support of this research.

References and Notes

(1) See, e.g.: De Vos, D. E.; Dams, M.; Sels, B. F.; Jacobs, P. A. *Chem. Rev.* **2002**, *102*, 3615−3640.

(2) Rolison, D. R. *Science* **2003**, *299*, 1698−1701.

(3) See, e.g.: Martin, P. J. In *Introduction to Molecular Electronics*; Petty, M. C., Bryce, M. R., Bloor, D., Eds.; Oxford: New York, 1995; pp 112−141.

(4) Ping, G.; Yuan, J. M.; Vallieres, M.; Dong, H.; Sun, Z.; Wei, Y.; Li, F. Y.; Lin, S. H. *J. Chem. Phys.* **2003**, *118*, 8042−8048. Friedel, M.; Sheeler, D. J.; Shea, J.-E. *J. Chem. Phys.* **2003**, *118*, 8106−8113.

(5) Jorgensen, W. L.; Binning, R. C., Jr.; Bigot, B. *J. Am. Chem. Soc.* **1981**, *103*, 4393−4399. Jorgensen, W. L. *J. Phys. Chem.* **1983**, *87*, 5304−5314. Jorgensen, W. L. *J. Am. Chem. Soc.* **1981**, *103*, 677−679.

(6) Scarsi, M.; Apostolakis, J.; Caflisch, A. *J. Phys. Chem. B* **1998**, *102*, 3637−3641.

(7) Tanabe, K. *Spectrochim. Acta, Part A* **1972**, *28A*, 407−424.

(8) Kato, M.; Abe, I.; Taniguchi, Y. *J. Chem. Phys.* **1999**, *110*, 11982−11986.

(9) Meléndez-Pagán, Y.; Taylor, B. E.; Ben-Amotz, D. *J. Phys. Chem. B* **2001**, *105*, 520−526.

(10) Bigot, B.; Costa-Cabral, B. J.; Rivail, J. L. *J. Chem. Phys.* **1985**, *83*, 3083−3094.

(11) Wong, M. W.; Frisch, M. J.; Wiberg, K. B. *J. Am. Chem. Soc.* **1991**, *113*, 4776−4782.
(12) Benjamin, I.; Pohorille, A. *J. Chem. Phys.* **1993**, *98*, 236−242.
(13) Wiberg, K. B.; Keith, T. A.; Frisch, M. J.; Murcko, M. *J. Phys. Chem.* **1995**, *99*, 9072−9079.
(14) Jorgensen, W. L.; McDonald, N. A.; Selmi, M.; Rablen, P. R. *J. Am. Chem. Soc.* **1995**, *117*, 11809−11810.
(15) Depaepe, J.-M.; Ryckaert, J.-P. *Chem. Phys. Lett.* **1995**, *245*, 653−659.
(16) Vilaseca, E. *J. Chem. Phys.* **1996**, *104*, 4243−4257.
(17) Herrebout, W. A.; van der Veken, B. J. *J. Phys. Chem.* **1996**, *100*, 9671−9677.
(18) Vilaseca, E. *Mol. Phys.* **1999**, *97*, 667−676.
(19) Madurga, S.; Vilaseca, E. *J. Phys. Chem. A* **2004**, *108*, 8439−8447.
(20) Zhang, J.; Jonas, J. *J. Phys. Chem.* **1993**, *97*, 8812−8815. Korb, J.-P.; Xu, S.; Jonas, J. *J. Chem. Phys.* **1993**, *98*, 2411−2422. Korb, J.-P.; Malier, L.; Cros, F.; Xu, S.; Jonas, J. *Phys. Rev. Lett.* **1996**, *77*, 2312−2315. Korb, J.-P.; Xu, S.; Cros, F.; Malier, L.; Jonas, J. *J. Chem. Phys.* **1997**, *107*, 4044−4050.
(21) Streck, C.; Mel'nichenko, Y. B.; Richert, R. *Phys. Rev. B* **1996**, *53*, 5341−5347. Richert, R. *Phys. Rev. B* **1996**, *54*, 15762−15766.
(22) Riter, R. E.; Willard, D. M.; Levinger, N. E. *J. Phys. Chem. B* **1998**, *102*, 2705−2714. Pant, D.; Riter, R. E.; Levinger, N. E. *J. Chem. Phys.* **1998**, *109*, 9995−10003. Riter, R. E.; Undiks, E. P.; Kimmel, J. R.; Levinger, N. E. *J. Phys. Chem. B* **1998**, *102*, 7931−7938. Willard, D. M.; Riter, R. E.; Levinger, N. E. *J. Am. Chem. Soc.* **1998**, *120*, 4151−4160. Willard, D. M.; Levinger, N. E. *J. Phys. Chem. B* **2000**, *104*, 11075−11080. Pant, D.; Levinger, N. E. *Langmuir* **2000**, *16*, 10123−10130. Riter, R. E.; Undiks, E. P.; Levinger, N. E. *J. Am. Chem. Soc.* **1998**, *120*, 6062−6067. Riter, R. E.; Kimmel, J. R.; Undiks, E. P.; Levinger, N. E. *J. Phys. Chem. B* **1997**, *101*, 8292−8297.
(23) Bhattacharyya, K.; Bagchi, B. *J. Phys. Chem. A* **2000**, *104*, 10603−10613.
(24) Sarkar, N.; Das, K.; Datta, A.; Das, S.; Bhattacharyya, K. *J. Phys. Chem.* **1996**, *100*, 10523−10527.
(25) Pal, S. K.; Sukul, D.; Mandal, D.; Sen, S.; Bhattacharyya, K. *J. Phys. Chem. B* **2000**, *104*, 2613−2616.
(26) Loughnane, B. J.; Fourkas, J. T. *J. Phys. Chem. B* **1998**, *102*, 10288−10294. Loughnane, B. J.; Scodinu, A.; Fourkas, J. T. *J. Phys. Chem. B* **1999**, *103*, 6061−6068. Loughnane, B. J.; Farrer, R. A.; Scodinu, A.; Reilly, T.; Fourkas, J. T. *J. Phys. Chem. B* **2000**, *104*, 5421−5429. Farrer, R. A.; Fourkas, J. T. *Acc. Chem. Res.* **2003**, *36*, 605−612.
(27) Wang, H.; Bardo, A. M.; Collinson, M. M.; Higgins, D. A. *J. Phys. Chem. B* **1998**, *102*, 7231−7237. Mei, E.; Bardo, A. M.; Collinson, M. M.; Higgins, D. A. *J. Phys. Chem. B* **2000**, *104*, 9973−9980.
(28) Zhang, J.; Bright, F. V. *J. Phys. Chem.* **1991**, *95*, 7900−7907.
(29) Cho, C. H.; Chung, M.; Lee, J.; Nguyen, T.; Singh, S.; Vedamuthu, M.; Yao, S.; Zhu, J.-B.; Robinson, G. W. *J. Phys. Chem.* **1995**, *99*, 7806−7812.
(30) Hara, K.; Kuwabara, H.; Kajimoto, O. *J. Phys. Chem. A* **2001**, *105*, 7174−7179.
(31) Hazra, P.; N. Sarkar, N. *Chem. Phys. Lett.* **2001**, *342*, 303−311.
(32) Luo, R.-S.; Jonas, J. *J. Raman Spectrosc.* **2001**, *32*, 975−978.
(33) Baumann, R.; Ferrante, C.; Deeg, F. W.; Bräuchle, C. *J. Chem. Phys.* **2001**, *114*, 5781−5791. Baumann, R.; Ferrante, C.; Kneuper, E.; Deeg, F. W.; Bräuchle, C. *J. Phys. Chem. A* **2003**, *107*, 2422−2430.
(34) Brown, D.; Clarke, J. H. R. *J. Phys. Chem.* **1988**, *92*, 2881−2888.
(35) Linse, P. *J. Chem. Phys.* **1989**, *90*, 4992−5004. Linse, P.; Halle, B. *Mol. Phys.* **1989**, *67*, 537−573.
(36) Faeder, J.; Ladanyi, B. M. *J. Phys. Chem. B* **2000**, *104*, 1033−1046. Faeder, J.; Ladanyi, B. M. *J. Phys. Chem. B* **2001**, *105*, 11148−11158.
(37) Senapati, S.; Chandra, A. *J. Chem. Phys.* **1999**, *111*, 1223−1230. Senapati, S.; Chandra, A. *J. Phys. Chem. B* **2001**, *105*, 5106−5109.
(38) Laria, D.; Kapral, R. *J. Chem. Phys.* **2002**, *117*, 7712−7718.
(39) Li, S.; Shepherd, T. D.; Thompson, W. H. *J. Phys. Chem. A* **2004**, *108*, 7347−7355.
(40) Thompson, W. H. *J. Chem. Phys.* **2002**, *117*, 6618−6628.
(41) Gomez, J.; Thompson, W. H. *J. Phys. Chem. B* **2004**, *108*, 20144−20154.
(42) Li, S.; Thompson, W. H. *J. Phys. Chem. B* **2005**, *109*, 4941−4946.
(43) Thompson, W. H. *J. Chem. Phys.* **2004**, *120*, 8125−8133.
(44) Thompson, W. H. In preparation.
(45) Mizushima, S. *Structure of Molecules and Internal Rotation*; Academic Press: New York, 1954.
(46) In the calculations presented here we have used a mass for the methylene groups in 1,2-dichloroethane corresponding to CHD. However, we have verified for 10 Å cavities that the free energy surfaces are only changed very slightly (<0.4 kcal/mol) compared to calculations using the mass of CH_2 and no qualitative features are changed.
(47) The volume used for calculating the densities is obtained by reducing the radius by $0.5\sigma_{Wall}$.
(48) Allen, M. P.; Tildesley, D. J. *Computer Simulation of Liquids*; Oxford University Press: New York, 1987.
(49) Frenkel, D.; Smit, B. *Understanding Molecular Simulation, from Algorithms to Applications*; Academic Press: New York, 1996.
(50) Kumar, S.; Bouzida, D.; Swendsen, R. H.; Kollman, P. A.; Rosenberg, J. M. *J. Comput. Chem.* **1992**, *13*, 1011−1021. Kumar, S.; Bouzida, D.; Swendsen, R. H.; Kollman, P. A.; Rosenberg, J. M. *J. Comput. Chem.* **1995**, *16*, 1339−1350.
(51) Torrie, G. M.; Valleau, J. P. *J. Comput. Phys.* **1977**, *23*, 187−199.